CAMERA CALIBRATION APPROACHES
USING SINGLE IMAGES OF MAN-MADE OBJECTS

L. Grammatikopoulos [a], G. E. Karras [a], E. Petsa [b]

[a] Department of Surveying, National Technical University of Athens, GR-15780 Athens, Greece (lazaros, gkarras@central.ntua.gr)
[b] Department of Surveying, Technological Educational Institute of Athens, GR-12210 Athens, Greece (petsa@teiath.gr)

KEY WORDS: Non-Metric, Calibration, Orientation, Single-Image Techniques, Geometry, Algorithms, Accuracy

ABSTRACT

Single image techniques may be very useful for heritage documentation purposes, not only in the particular instances of damaged or destroyed objects but also as auxiliary means for a basic metric reconstruction. In the general case, single images have unknown interior orientation, thus posing the fundamental question of camera calibration (as in several cases no ground control is available). To this end, the known – or assumed – geometry of imaged man-made objects may be exploited. Recovery of the three main elements of interior orientation, together with image attitude, requires the existence on the image of lines in three known non-coplanar directions, typically orthogonal to each other (from the lines, radial lens distortion might also be estimated). Several approaches have been reported for the exploitation of this basic image geometry; however, the expected accuracy has not been adequately investigated. In this contribution, three alternative algorithms are presented, based: on the direct use of the three basic image vanishing points; on the use of image line parameters; and on the direct use of image point observations. The integration of radial distortion into the algorithms is also presented. The reported results are evaluated, and promising conclusions are drawn regarding the performance and limitations of such camera calibration methods, as compared to self-calibrating bundle adjustment techniques based on control points.

1. INTRODUCTION

Under certain circumstances photogrammetry is asked to handle documentation questions for cultural items partly or totally damaged. So, it happens that old ('historic') images can be the exclusive source for metric information; these may well be single amateur photographs. Not taken for photogrammetric purposes, they usually lack control information or camera data. Fortunately enough, however, man-made objects usually contain straight lines, thus being suitable for methods of line photogrammetry.

But single-image line photogrammetry is evidently not restricted to old images; its uses include very diverse tasks like vehicle or robot navigation and metric exploitation of surveillance cameras (topics extensively studied in the field of computer vision). In fact, what is more important is an understanding of the underlying image geometry, common to all monoscopic techniques. For the purposes of this contribution, a single-image approach may be regarded as consisting of three, albeit not independent, steps: camera calibration; image orientation; object reconstruction.

Regarding 1D measurements, one suitable vanishing point on an uncalibrated image may be sufficient (Grammatikopoulos et al., 2002). For 2D objects, e.g. planar facades, two vanishing points of known angle permit to recover image rotations and the camera constant, and hence rectification (Karras et al., 1993). But if the principal point cannot be ignored, rectification requires further information (a length proportion). Regarding 3D structures, Gracie (1968) has derived all necessary equations for estimating interior orientation parameters and camera attitude in a configuration with three vanishing points in orthogonal directions. Results have been reported with this approach by both Bräuer-Burchardt & Voss (2001) and Petsa et al. (2001) regarding old photographs (the former also address cases where one of the vanishing points is close to infinity by using appropriate length ratios). To the same effect, van den Heuvel (2001) adjusted line observations with constraints among lines for camera calibration.

Unlike approaches founded on vanishing points, Petsa & Patias (1994) had presented an algorithm using image line parameters, estimated previously; these are subsequently adjusted to recover

interior orientation and rotation matrix. This approach has been successfully applied to uncalibrated photographs of both existing buildings and a torn down theatre (Karras & Petsa, 1999).

Here, the particular problem of camera calibration is addressed. Besides being a step towards the final goal of reconstruction, it constitutes a problem in its own right: How reliable are simple single-image calibration approaches, which do not rely on conventional control information but, merely, on object geometry? Here, different formulations are discussed and evaluated against a rigorous multi-image bundle adjustment approach.

In most instances, radial lens distortion is either neglected or is estimated beforehand (as in Bräuer-Burchardt & Voss, 2001) by one of the simple methods at hand (Karras & Mavromati, 2001). Here, radial distortion has also been introduced into the algorithms to allow camera calibration in one single step.

2. ALTERNATIVE FORMULATIONS

2.1 Use of vanishing points

As mentioned already, Gracie (1968) has given the formulae for determining the three interior orientation elements (camera constant c and principal point x_o, y_o) and the three ω, φ, κ image rotations from the vanishing points of three orthogonal directions, which provide the six necessary equations. Thus, the adjustment refers here to the estimation of vanishing points from individual point measurements x_i, y_i on converging image lines. The fitted lines are constrained to converge to the corresponding vanishing point $F(x_F, y_F)$ according to following observation equation:

$$x_i - x_F - (y_i - y_F) t = 0 \qquad (1)$$

According to line direction, the equation can be also formulated using slope $t = \Delta y / \Delta x$ with respect to the x-axis. Having estimated vanishing point locations, subsequent determination of interior orientation elements and rotation matrix **R** is then straightforward. This is approach A.

In Eq. (1), radial symmetric lens distortion Δr has been ignored. It can be introduced as follows:

$$x_i - (x_i - x_o)(k_1 r^2 + k_2 r^4) - x_F - \\ -\left[y_i - (y_i - y_o)(k_1 r^2 + k_2 r^4) - y_F \right] t = 0 \qquad (2)$$

In this case, all point observations are adjusted in one step, with common unknowns the two distortion coefficients (k_1, k_2). If it cannot be assumed that the principal point, about which distortion is assumed to be radial-symmetric, is near the image centre, then a first solution without distortion is required to provide an adequate estimate for its location as regards distortion. Finally, let it be noted that the mean standard error of unit weight (σ_o) from the adjustments for the three vanishing points is a measure for the precision of the adjustment.

2.2 Use of line elements

In this case, the basic mathematical model, given in Petsa & Patias (1994), could be summarised as follows. Let G be an object line and ε the central projection plane of corresponding image line g. Further, let $\mathbf{n}$ be the normal vector of ε and $\boldsymbol{\delta}^t = [L\ M\ N]$ the direction vector of the object line. If $\mathbf{R}$ denotes the matrix of image rotations, then

$$\mathbf{n}^t \mathbf{R} \boldsymbol{\delta} = 0 \qquad (3)$$

is the condition for the orthogonality of the two vectors $\mathbf{n}$ and $\boldsymbol{\delta}$. This is equivalent to the parallelism of space line G (and, hence, of all object lines of the same direction) with projection plane ε (and, hence, all projection planes of object lines of direction $\boldsymbol{\delta}$). The vector $\mathbf{n}$ is a function of the three interior orientation parameters and image line elements. Regarding the latter, two alternative formulations are possible, giving rise to two different approaches.

In the first case, it is line parameters that are considered as observations to be adjusted; in the other case, all individual point measurements on all image lines are treated as observations.

Use of image line parameters as observations

Here, as formulated in Petsa & Patias (1994), parameters a, b of the 'intercept form' of image lines

$$\frac{x}{a} + \frac{y}{b} + 1 = 0 \qquad (4)$$

are assumed to be known after individual line fitting. Vector $\mathbf{n}$ is then a function of interior orientation and line parameters:

$$\mathbf{n}^t = \begin{bmatrix} -cb & -ca & ab + bx_o + ay_o \end{bmatrix} \qquad (5)$$

Setting

$$\mathbf{R}\boldsymbol{\delta} = \begin{bmatrix} U & V & W \end{bmatrix} \qquad (6)$$

and introducing Eqs. (5) and (6) into Eq. (3), finally results in

$$cbU + caV - (ab + bx_o + ay_o)W = 0 \qquad (7)$$

Every object line of known direction gives rise to one orthogonality condition (7). Image lines are first fitted and subsequently carried into the adjustments as observations, weighted by means of their variance-covariance matrix. This is approach B.

Thus, contrary to method A, here a two-step process is adopted. First, points are simply constrained on lines (lens distortion can be estimated along with the line parameters); next, line parameters are introduced into the perspective equations (7) to recover the values of the involved parameters c, x_o, y_o and ω, φ, κ. This approach has been reformulated here in a more rigorous one-step procedure, as follows.

Use of image point measurements as observations

In this case, an image line is expressed by each of its individual points and the line slope, assumed as $t = \Delta x / \Delta y$ (under certain circumstances the equivalent formulation with $t = \Delta y / \Delta x$ may be required). Thus, Eq. (5) takes the following form:

$$\mathbf{n}_i^t = \begin{bmatrix} c & -ct & (x_i - x_o) - (y_i - y_o)t \end{bmatrix} \qquad (8)$$

Accordingly, using again the quantities of Eq. (6), Eq. (3) finally becomes:

$$cU - ctV + \left[(x_i - x_o) - (y_i - y_o)t \right] W = 0 \qquad (9)$$

All measured image points x_i, y_i on all lines contribute one such condition to the adjustment. Hence, line fitting, camera calibration and image orientation are performed in one single step. The standard error of unit weight σ_o provides the precision estimate for the adjustment. This is approach C.

The coefficients of radial lens distortion can also be incorporated into the solution, as follows:

$$cU - ctV + \left[(x_i - x_o) - (y_i - y_o)t \right]\left(1 - k_1 r^2 - k_2 r^4\right)W = 0 \quad (10)$$

Using Eq. (10) for every observed image point, it is possible to estimate simultaneously the 8 involved parameters (c, x_o, y_o, k_1, k_2; ω, φ, κ) along with the slopes t_i of all image lines. Of course, such an adjustment might be somewhat sensitive regarding estimation of distortion, as it depends on length and distribution (as well as noise) of measured image line segments. Yet, in the performed tests estimation of distortion was in accordance with the results from self-calibrating bundle adjustment (see 3.3 below).

Concluding the presentation of mathematical models, it is noted that approaches A and C are indeed straightforward, as the raw observations (namely, points on image lines) are adjusted in one single step under the constraint of central projection (in case A, the unknowns are then directly extracted from an equal number of equations). In this sense, approach B differs since the raw observations are initially subject only to a linearity constraint, and line parameters thus obtained become in fact the 'fictitious' observations in the final adjustment step (hence, weighting is here indispensable).

3. PRACTICAL INVESTIGATIONS

In the first tests, objects with no ground control were used. The purpose was to check the performance of the algorithms and the agreement of their results. In the next series of investigations, the results for a known 3D object were evaluated in relation to a multi-image bundle adjustment.

3.1 Results from the different single-image approaches

The eight images used here, seen in Fig. 1, had been taken with

small format analogue cameras, using different lenses (35 mm; 50 mm; the extremes of a 24–45 mm zoom lens). Since the enlarged prints had been somewhat cropped, the interest focused here not on the actual values of interior orientation but rather on the closeness of results from the three calibration approaches (it is noted that the images were scanned in different resolutions).
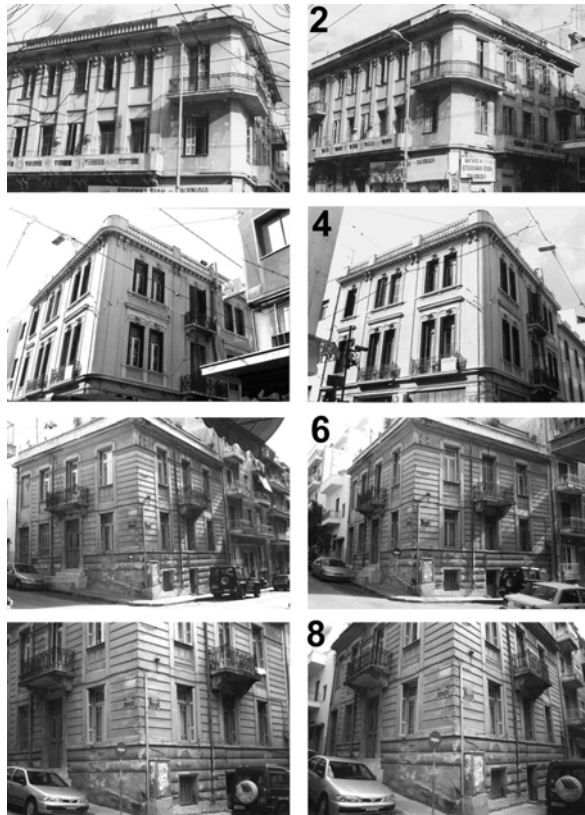

Figure 1. The images of the first test.

Table1. Results of single image calibrations					
Image	Method	c (mm)	x_o (mm)	y_o (mm)	σ_o
1 *50 mm*	A	48.84	−1.34	−2.30	7.6 μm
	C	48.80 ± 0.16	−1.28 ± 0.15	−2.32 ± 0.09	7.6 μm
	B	48.84 ± 0.21	−1.26 ± 0.20	−2.50 ± 0.12	1.5
2 *50 mm*	A	48.89	0.63	−2.06	7.1 μm
	C	48.89 ± 0.13	0.66 ± 0.26	−2.08 ± 0.12	7.0 μm
	B	48.69 ± 0.20	0.77 ± 0.36	−2.08 ± 0.26	1.9
3 *35 mm*	A	35.16	0.63	−1.31	8.8 μm
	C	35.16 ± 0.05	0.63 ± 0.06	−1.32 ± 0.05	9.1 μm
	B	35.13 ± 0.13	0.52 ± 0.20	−1.33 ± 0.12	2.9
4 *35 mm*	A	34.66	0.56	−1.11	9.4 μm
	C	34.66 ± 0.05	0.56 ± 0.06	−1.12 ± 0.05	9.4 μm
	B	34.63 ± 0.09	0.56 ± 0.10	−1.21 ± 0.09	2.6
5 *35 mm*	A	36.05	−1.30	0.62	17.4 μm
	C	36.05 ± 0.12	−1.24 ± 0.26	0.52 ± 0.15	17.6 μm
	B	36.16 ± 0.27	−1.76 ± 0.58	0.75 ± 0.40	3.3
6 *35 mm*	A	35.69	−0.08	1.03	16.3 μm
	C	35.69 ± 0.12	−0.20 ± 0.20	1.06 ± 0.16	16.5 μm
	B	36.10 ± 0.23	−0.14 ± 0.41	1.22 ± 0.28	3.2
7 *45 mm*	A	43.42	−0.12	1.28	17.7 μm
	C	43.42 ± 0.14	−0.14 ± 0.26	1.19 ± 0.13	16.9 μm
	B	43.92 ± 0.55	0.61 ± 0.81	1.29 ± 0.46	5.8
8 *24 mm*	A	24.46	−0.20	1.82	19.5 μm
	C	24.49 ± 0.07	−0.19 ± 0.12	1.79 ± 0.07	19.7 μm
	B	24.40 ± 0.17	0.07 ± 0.24	1.85 ± 0.14	2.6

Results from all three approaches, whereby radial distortion has been ignored, are presented in the above Table 1. It is clear that approaches A and C give values for calibration parameters practically identical; the same holds true for the precision estimates σ_o (regarding approach B, it is noted that σ_o is dimensionless as the observations are actually weighted). Thus, it appears that indeed these two methods are essentially equivalent. Approach B, on the other hand, gives similar results for the first 4 images, for which small σ_o values are present; yet, significant deviations do exist in some of the remaining images (for instance, differences in c reaching 1.1%), where σ_o values are large. This could be an indication that, since line fitting is performed as a separate step, this method might be more sensitive to 'noise'.

The last remark to be made here is that the precision of the unknowns, too, appears to be considerably smaller in approach B than in C. It is noted that in method A, where the unknowns are finally found with no redundancy, precision estimations for the camera parameters could also be calculated as an error propagation of vanishing point standard errors, emerging from the line fitting adjustment using Eq. (1), to the values of interior orientation parameters.

3.2 Comparison of single-image and multi-image approaches

In this case, a regular grid was used to provide ample control. A number of toy items had been placed on it to create a 3D object, but also to provide vertical control. This structure has then been recorded ten times using a KODAK DCS420 camera (1524×1012 pixels of size 9.2 μm) and a 28 mm lens. Thus, the performance of single-image approaches was assessed under rather unfavourable conditions due to the weak perspective of the narrow-angle lens.

Six images (shown in Fig. 2) were selected for the single-image tests, namely those whose converging lines did not intersect at exceedingly small angles in any of the three vanishing points. These same six images were used in the bundle adjustments.
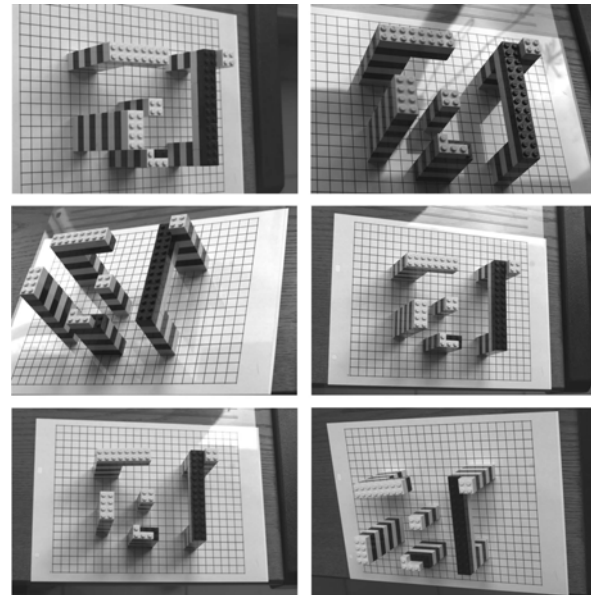

Figure 2. The images of the second test.

A self-calibrating bundle solution was carried out (ignoring distortion) with all six images, based on a total of 25 control points (21 full and 4 vertical) and 60 tie points. Regarding the single-image calibrations, 3 image lines were measured in the grid X,Y

directions; more lines (7–13) were measured in the direction of depth, to compensate for short line segments. After solution, the values of interior orientation parameters from each approach for each image were consecutively introduced into the bundle of six images as fixed camera parameters.

For all 18 bundle solutions, deviations d_X, d_Y, d_Z of all estimated tie point coordinates from their known values were calculated, to provide the mean absolute deviations d for all solutions. This allows assessing the effectiveness of single-image pre-calibration using lines. The results are seen in Table 2, in which the first row gives the outcome of self-calibration.

Table 2. Calibration results from single images
and from bundle adjustment using 6 images
*d: mean absolute deviation of tie points from bundle adjustments
using the calibration results from single images as fixed*

Image	Method	c (mm)	x_o (mm)	y_o (mm)	σ_o	d (mm)
	Bundle	30.06	−0.18	−0.07	4.4 μm	0.09
1	A	30.53	−0.54	0.05	6.4 μm	0.09
	C	30.55	−0.60	0.00	5.7 μm	0.10
	B	30.37	−0.12	0.04	3.2	0.09
2	A	30.67	−0.04	0.36	6.1 μm	0.10
	C	30.67	−0.04	0.37	6.3 μm	0.10
	B	30.81	0.00	0.48	3.2	0.11
3	A	30.68	0.43	0.61	5.4 μm	0.14
	C	30.68	0.42	0.62	5.3 μm	0.14
	B	30.82	0.46	0.81	3.1	0.15
4	A	30.79	−0.23	0.19	4.0 μm	0.09
	C	30.71	−0.19	0.15	3.8 μm	0.09
	B	31.91	−0.77	0.39	3.4	0.17
5	A	30.14	0.20	0.06	6.2 μm	0.11
	C	29.99	0.28	−0.03	5.2 μm	0.12
	B	30.63	0.05	0.26	3.5	0.10
6	A	30.72	0.80	−0.38	6.0 μm	0.17
	C	30.74	0.81	−0.38	5.2 μm	0.17
	B	29.76	0.26	−0.10	4.9	0.12

Here again, approaches A and C yield very similar results. It is also seen that all approaches display considerable deviations regarding the camera constant, whose values consistently exceed those of the bundle approach. The values for the principal point, too, show large fluctuations. However, it is basically not advisable to directly compare parameter values from adjustments differing in input data and/or algorithm. Generally, in bundle solutions the camera parameter values are tightly correlated with the exterior orientation parameters of several images (for instance, the adjustments of the 6 images and of all 10 images gave a difference of $\Delta c = 0.15$ mm for the camera constant).

Thus, object reconstruction with the different camera parameter values would probably be more reliable for assessing the different approaches. In Table 2 it is clearly seen that, for the camera parameter values obtained from individual images with all three approaches, the mean absolute differences d (representing accuracy of the intersected object points) are at most about 1.6 times larger than those from the self-calibrating bundle solution. One exception exists in each case (image 6 for approaches A, C and image 4 for B), with d still being less than 2 times larger.

It may be concluded that, in the present case, single-image camera calibration from linear features results in at most doubling inaccuracy as compared to self-calibration. This, of course, is an overall assessment, since approach B appears to behave differently regarding the individual images.

3.3 Including radial lens distortion in the adjustments

In the preceding tests, lens distortion Δr has been ignored. Now, it has been included among the unknowns, using Eqs. (2) and (10) for approaches A and C, respectively. Further, Δr has also been estimated in a bundle solution using all images. Again, the values for the camera parameters of each image obtained from both methods have been introduced, successively, as fixed data on camera geometry into the bundle adjustment.

The results for distortion, obtained with approach A, are seen in Fig. 3 (distortion curves from approach C are almost identical). It is clear that here single-image solutions provide a satisfactory estimation of radial lens distortion.
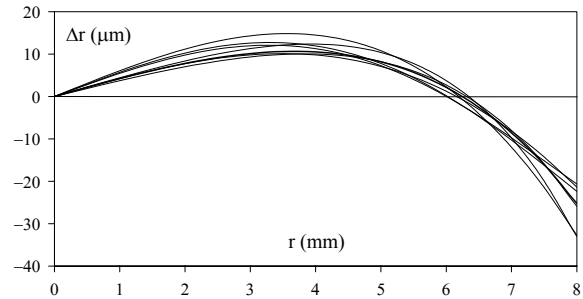

Figure 3. Calibrated distortion curves from bundle solution (dark line) and from vanishing point estimation using Eq. (2).

The results for camera calibration and object reconstruction are shown in Table 3. In comparison to Table 2, the precision of adjustments (σ_o values) has improved considerably thanks to the correction of distortion; the same holds true for the mean absolute differences (d) of tie points.

Table 3. Calibration results from single images and bundle adjustment with estimation of radial distortion

Image	Method	c (mm)	x_o (mm)	y_o (mm)	σ_o	d (mm)
	Bundle	30.06	−0.06	−0.07	3.5 μm	0.05
1	A	30.47	0.71	0.07	4.9 μm	0.09
	C	30.60	1.58	0.03	4.9 μm	0.11
2	A	30.62	0.19	0.33	5.3 μm	0.06
	C	30.67	0.26	0.45	5.3 μm	0.07
3	A	30.38	−0.19	0.31	4.4 μm	0.06
	C	30.52	−0.27	0.56	4.4 μm	0.07
7	A	30.76	0.32	0.22	3.4 μm	0.07
	C	30.79	0.42	0.26	3.4 μm	0.02
8	A	30.11	−0.10	0.04	4.8 μm	0.05
	C	30.11	−0.13	0.12	4.8 μm	0.05
11	A	30.54	−0.60	−0.32	4.9 μm	0.09
	C	30.72	−0.87	−0.42	4.9 μm	0.12

Otherwise, similar remarks as before may be made. Differences in camera constant remain large, and so does the scatter of the principal point coordinates. Yet, object point errors from single-image approaches hardly exceed the corresponding value from bundle solution by a factor of about 2.

4. DISCUSSION

Here, mathematical models for single image calibration, relying on measurements of straight lines in three orthogonal directions, have been presented and assessed against bundle adjustment. As it is, generally, rather unwise to directly compare parameter data from different sources, evaluation has relied on the use of

camera information derived from lines as fixed values in bundle solutions. Results indicate that, at least in this case, such techniques lead to 'reasonable' errors, about twice as large as those of a rigorous solution. In this sense, they could be used when bundle solutions are impossible or impracticable. Lens distortion, too, can apparently be estimated satisfactorily by means of such one-step single-image methods.

Of course, a more conclusive evaluation requires further investigations with various lenses, notably wide-angle, but also regarding the limits of application of these approaches with respect to length and distribution of image line segments, noise and image rotations. The presented results, nonetheless, indicate in practical terms that these approaches do have the potential for camera calibration and, hence, the next steps of object reconstruction.

REFERENCES

Bräuer-Burchardt, C., Voss, K., 2001. Façade reconstruction of destroyed buildings using historical photographs. *XVIII CIPA International Symposium*, Potsdam, pp. 543-550.

Gracie, G., 1968. Analytical photogrammetry applied to single terrestrial photograph mensuration. *XI Congress of the International Society for Photogrammetry*, Lausanne, 8-20 July.

Grammatikopoulos, L., Karras, G., Petsa, E., 2002. Geometric information from single uncalibrated images of roads. *Int. Arch. Phot. & Rem. Sens.*, 34(5), pp. 21-26.

Karras, G., Patias, P., Petsa, E. 1993. Experiences with digital rectification on non-metric images when ground control is not available. *XV CIPA International Symposium*, Bucharest (proceedings in print).

Karras, G., Petsa, E., 1999. Metric information from single uncalibrated images. *XVII CIPA International Symposium*, Olinda, (proceedings in CD)

Karras, G., Mavromati, D., 2001. Simple calibration techniques for non-metric cameras. *XVIII CIPA International Symposium*, Potsdam, pp. 39-46.

Petsa E., Patias P., 1994. Formulation and assessment of straight line based algorithms for digital photogrammetry. *Int. Arch. Phot. Rem. Sens.,* 30(5), pp. 310-317.

Petsa, E., Kouroupis, S., Karras, G., 2001. Inserting the past in video sequences. *XVIII CIPA International Symposium*, Potsdam, pp. 707-712.

van den Heuvel, F.A., 2001. Reconstruction from a single architectural image from the Meydenbauer Archives. *CIPA XVIII International Symposium*, Potsdam, pp. 699-706.